

Morphological effect on electrochemical performance of nanostructural CrN

Zhengwei Xiong(熊政伟), Xuemei An(安雪梅), Qian Liu(刘倩), Jiayi Zhu(朱家艺), Xiaoqiang Zhang(张小强), Chenchun Hao(郝辰春), Qiang Yang(羊强), Zhipeng Gao(高志鹏), and Meng Zhang(张盟)

Citation: Chin. Phys. B, 2021, 30 (**12**): 128201. DOI: 10.1088/1674-1056/ac1f07
Journal homepage: http://cpb.iphy.ac.cn; http://iopscience.iop.org/cpb

What follows is a list of articles you may be interested in

Band alignment between NiO_x and nonpolar/semipolar GaN planes for selective-area-doped termination structure

Ji-Yao Du(都继瑶), Ji-Yu Zhou(周继禹), Xiao-Bo Li(李小波), Tao-Fei Pu(蒲涛飞), Liu-An Li(李柳暗), Xin-Zhi Liu(刘新智), and Jin-Ping Ao(敖金平)

Chin. Phys. B, 2021, 30 (**6**): 067701. DOI: 10.1088/1674-1056/abdb21

Fabrication and characterization of Ge–Ga–Sb–S glass microsphere lasers operating at~1.9 μm

Kun Yang(杨坤), Shixun Dai(戴世勋), Yuehao Wu(吴越豪), Qiuhua Nie(聂秋华)

Chin. Phys. B, 2018, 27 (**11**): 117701. DOI: 10.1088/1674-1056/27/11/117701

Low-temperature green synthesis of boron carbide using aloe vera

H V SarithaDevi, M S Swapna, G Ambadas, S Sankararaman

Chin. Phys. B, 2018, 27 (**10**): 107702. DOI: 10.1088/1674-1056/27/10/107702

Effect of oxygen content on dielectric characteristics of Cr-doped $LaTiO_x$

Ming Ma(马铭), Yan Chen(陈彦), Yi-Min Cui(崔益民)

Chin. Phys. B, 2018, 27 (**5**): 057702. DOI: 10.1088/1674-1056/27/5/057702

Wavy structures for stretchable energy storage devices: Structural design and implementation

Lei Wen(闻雷), Ying Shi(石颖), Jing Chen(陈静), Bin Yan(严彬), Feng Li(李峰)

Chin. Phys. B, 2016, 25 (**1**): 018207. DOI: 10.1088/1674-1056/25/1/018207

Morphological effect on electrochemical performance of nanostructural CrN*

Zhengwei Xiong(熊政伟)[1,†], Xuemei An(安雪梅)[4,†], Qian Liu(刘倩)[1], Jiayi Zhu(朱家艺)[1], Xiaoqiang Zhang(张小强)[2], Chenchun Hao(郝辰春)[1,‡], Qiang Yang(羊强)[3], Zhipeng Gao(高志鹏)[3], and Meng Zhang(张盟)[1]

[1] *Joint Laboratory for Extreme Conditions Matter Properties, Southwest University of Science and Technology, Mianyang* 621010, *China*
[2] *Institute of Electronic Engineering, China Academy of Engineering Physics (CAEP), Mianyang* 621900, *China*
[3] *Institute of Fluid Physics, China Academy of Engineering Physics, Mianyang* 621900, *China*
[4] *Affiliated Hospital, Chengdu University of Traditional Chinese Medicine, Chengdu* 611137, *China*

(Received 17 May 2021; revised manuscript received 10 August 2021; accepted manuscript online 19 August 2021)

Size and morphology are critical factors in determining the electrochemical performance of the supercapacitor materials, due to the manifestation of the nanosize effect. Herein, different nanostructures of the CrN material are prepared by the combination of a thermal-nitridation process and a template technique. High-temperature nitridation could not only transform the hexagonal Cr_2O_3 into cubic CrN, but also keep the template morphology barely unchanged. The obtained CrN nanostructures, including (i) hierarchical microspheres assembled by nanoparticles, (ii) microlayers, and (iii) nanoparticles, are studied for the electrochemical supercapacitor. The CrN microspheres show the best specific capacitance (213.2 F/g), cyclic stability (capacitance retention rate of 96% after 5000 cycles in 1-mol/L KOH solution), high energy density (28.9 Wh/kg), and power density (443.4 W/kg), comparing with the other two nanostructures. Based on the impedance spectroscopy and nitrogen adsorption analysis, it is revealed that the enhancement arised mainly from a high-conductance and specific surface area of CrN microspheres. This work presents a general strategy of fabricating controllable CrN nanostructures to achieve the enhanced supercapacitor performance.

Keywords: CrN, supercapacitors, metal nitride, nanostructures

PACS: 82.47.Uv, 77.74.Bw, 79.60.Jv, 91.60.Ed **DOI:** 10.1088/1674-1056/ac1f07

1. Introduction

Supercapacitor is an important energy-storage device, presenting a longer lifetime ($> 10^5$ cycles), high power density (> 10 mW/cm^2), and rapid charge/discharge capabilities safely. Nowsdays, commercial supercapacitors have been widely used in heavy-duty vehicles, load-leveling systems, and hybrid platforms. However, the common energy density of supercapacitors (~ 5 Wh/kg) was still lower than that of batteries (up to 200 Wh/kg) or fuel cells (up to 350 Wh/kg).[1] In the past decades, much efforts have been paid for improving the storage performance for supercapacitors. Transition metal nitrides (TMNs) were extensively investigated for many applications, such as electrocatalytic water splitting,[2] plasmonics,[3] and supercapacitors,[4] owing to their excellent conductivity, prominent thermal/chemical stability and outstanding electrochemical performance. Various TMNs, including nickel nitride,[5] titanium nitride,[6] vanadium nitride,[7,8] and molybdenum nitride,[9] have been explored as novel electrode materials for supercapacitors, showing superior specific capacitance and rate performance. In particular, chromium nitride (CrN) with a high resistance to wear and corrosion shows a promising advantage over conventional transition metal oxides in energy storage.[10–13] Lots of synthetic approaches to nanostructured CrN have been reported including physical vapor deposition, nanopatterning, and DC magnetron sputtering. Das *et al.* synthesized CrN nanoparticles with the size of 20 nm–30 nm by using the combination of a hydrothermal method and a nitridation process, showing a specific capacitance of 75 F/g at the current density of 30 mA/g.[11] Haye *et al.* prepared CrN films by magnetron sputtering at glancing angle (GLAD), and obtained a high areal capacitance of 35.4 mF/cm^2 at 1.2 mA/cm^2.[14] Wei *et al.* reported a high areal specific capacitance (12.8 mF/cm^2 at 10 mV/s) of CrN thin films prepared by DC magnetron sputtering technology, and the CrN thin film also exhibited high cycling stability with 92.1% capacitance retention after 2×10^4 cycles in the H_2SO_4 electrolyte (0.5 M).[10] However, the reported specific capacitance of CrN was still relatively low, as a disadvantage of TMNs based supercapacitor, comparing with metal oxides, mxenes or transition metal phosphides.[15]

The morphology and size are critical factors in determining the electrochemical performance of the supercapacitor ma-

*Project supported by the National Natural Science Foundation of China (Grant Nos. 11904299, U1930124, and 11804312) and China Academy of Engineering Physics (CAEP) Foundation (Grant No. 2018AB02).

†These authors contributed to this work equally.

‡Corresponding author. E-mail: haochenchun@swust.edu.cn

© 2021 Chinese Physical Society and IOP Publishing Ltd

terials with a single component, due to the manifestation of the nanosize effect. As we know, the morphology, size, and synthetic method of TMNs may remarkably improve the number of redox centers and enhance their supercapacitor performance. For example, two-dimensional nanomaterials with a large specific surface area facilitate interfacial reactions in supercapacitors, rechargeable batteries, as well as catalysts.[16] Due to the unique structure, the obtained free-standing TiN nanosheet arrays have a large specific capacitance of 81.63 F/g and excellent cycling performance without capacitance decay after 2500 cycles.[17] Huo *et al*. synthesized VN nanoflakes from nitriding V_2O_5 nanoflakes xerogel, resulting in the large nanoflake morphology of VN with porous structure. The VN material had a high specific capacitance of 152 F/g at 1 A/g in the alkaline solution.[18] However, the effect of morphology and size for the CrN material on the supercapacitor was rarely studied, as far as we know. Herien, three nanostructures of the CrN material were studies for their electrochemical properties in this work, basing on the Cr_2O_3 precursors with different morphologies. The obtained CrN nanostructures, including (i) hierarchical microspheres assembled by nanoparticles, (ii) microlayers, and (iii) nanoparticles, were prepared by the combination of a thermal-nitridation process and a template (Cr_2O_3) technique. As a result, high-temperature nitridation could not only transform the hexagonal Cr_2O_3 into cubic CrN completely, but also keep the template' morphology unchanged. The electrochemical performance of CrN nanostructures assembling into supercapacitors was systematically tested and discussed.

2. Experimental details

2.1. Preparation of Cr_2O_3 precursor

(i) The microspheres Cr_2O_3 precursor was synthesized by a modified hydrothermal method.[19] Briefly, 0.8-mmol glucose and 0.1-mmol $Cr(NO_3)_3{\cdot}9H_2O$ were dissolved in 40-ml and 20-ml deionized water, respectively. The two solutions were then mixed and placed in 100 ml of teflon liner coated with a stainless steel autoclave. After keeping the temperature at 180 °C for 24 h, a black precipitate was obtained. Then, the powders were washed with deionized water and alcohol three times, and dried in a drying oven at 60 °C for 5 h. Finally, the powders were heated up to 550 °C for 4 h in a muffle furnace at an atmosphere. (ii) The Cr_2O_3 microplates precursor was synthesized by a method reported previously.[20] Firstly, 15 mL of $Cr(NO_3)_3$ solution (0.1 mol/L) was heated to 70 °C under magnetic stirring. Then, the ammonia solution was added to the above solution dropwise, until the pH = 9. The suspension was kept at room temperature for 1 h. Finally, it was washed with deionized water, and then dried under reduced pressure at 140 °C in a drying cabinet. (iii) The Cr_2O_3 nanoparticle precursor was synthesized by a simple annealing method. Firstly, 1 mmol of $CrCl_3{\cdot}6H_2O$ and 3 mmol of propylene oxide were stirred in 40 mL of DI water in a breaker to form a gel. Then, the obtained gel was placed in an aluminum oxide crucible, and heated to 600 °C. The state was kept for 1 hour in the atmosphere, and the product was obtained.

2.2. Preparation of CrN nanostructures

By using the above-mentioned three Cr_2O_3 precursors with different morphologies, we obtained three different nanostructural CrNs respectively. Briefly, 2.0 g of the above three kinds of Cr_2O_3 powders were loaded into a crucible, respectively, and heated to 800 °C in an ammonia (NH_3) atmosphere. The NH_3 flow rate was 0.06 m^3/h, and the process was kept for 4 h. Then, the system was naturally cooled to room temperature. Note that NH_3 was introduced for 0.5 h before the temperature rise, ensuring that the air in the furnace was fully eliminated. The generated tail gas was absorbed by dilute H_2SO_4 solution. The schematic diagram of CrN preparation was shown in Fig. 1.

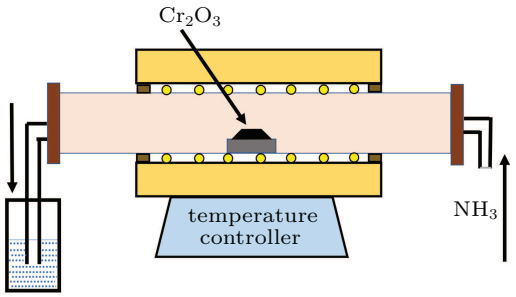


Fig. 1. Schematic diagram of CrN fabrication.

2.3. Structure characterization

All the samples used an x-ray diffractometer (XRD) to test the crystal structure of the material. The x-ray source is Cu target $K\alpha$ radiation ($\lambda = 0.154$ nm), the 2θ measuring range is 10°–80°, and the scanning rate is 8 °/min. The micromorphology of the samples was observed at high magnifications such as 10^4 (10 kx) and 5×10^4 (50 kx) with a high-resolution cold field emission scanning electron microscope (SEM). The chemical bond composition of the products was characterized by x-ray electron spectroscopy (XPS). A transmission electron microscope (TEM) with high-resolution transmission electron microscope (HRTEM) was used to observe the internal structure of the samples. With the Asap2020 chemical adsorption analyzer, the specific surface area of the sample was calculated by the Brunauer–Emmett–Teller (BET) equation of N_2 adsorption isotherm.

2.4. Electrochemical characterization

The working electrode was fabricated by a slurry-forging method with Ti sheet electrode. Briefly, CrN powders, conductive carbon powders, and polyvinylidene fluoride (PVDF) were mixed uniformly with a mass ratio of 8:1:1. Then,

they were added with the N-methylpyrrolidone (NMP) until the mixed powder is ground into a thick slurry. The paste was uniformly coated on one side of the cleaned Ti sheet electrode and then dried in a drying box at 40 °C for 12 h. The cyclic voltammetry curve (CV), constant current charge-discharge curve (GCD), impedance spectroscopy (EIS), and cyclic voltammetry stability of the CrN electrode material were tested through the electrochemical workstation (CHI660E) with a three-electrode system. The as-prepared CrN electrode, Hg/HgO and Pt sheets were used as working electrodes, the reference electrode, and the counter electrode, respectively. The electrolyte was 1-mol/L KOH. According to the CV and GCD curves, the specific capacitance (C_s) of the electrode material could be calculated separately by

$$C_s = \frac{\int I \mathrm{d}V}{2mv\Delta V}, \tag{1}$$

$$C_s = \frac{I\Delta t}{m\Delta V}, \tag{2}$$

where I is current, m is the material quality, ΔV is the voltage window during the test, v is the scan rate of the CV curves, and Δt is the discharge time. The energy density (E) and power density (P) of the CrN electrode materials was calculated by the following equations

$$E = \frac{C_s \Delta v^2}{2}, \tag{3}$$

$$P = \frac{E}{\Delta t}, \tag{4}$$

where ΔV and Δt are the voltage window and time of discharge, respectively.

3. Results and discussion

First, nanostructural Cr_2O_3 precursors were synthesized with three kind of morphologies with nanoparticles, microlayer, and microsphere. The Cr_2O_3 nanoparticles were generated by high-temperature sintering of the gel formed by chromium trichloride hexahydrate and propylene oxide. Dispersed nanoparticles were found with a relatively uniform size (Figs. 2(a) and 2(b)). The microlayered Cr_2O_3 was obtained by drying chromium nitrate solution under reduced pressure in an alkaline environment (Figs. 2(c) and 2(d)). Its surface was composed of Cr_2O_3 nanoparticles bonded and stacked. Importantly, the microspherical Cr_2O_3 was prepared by a reported hydrothermal method, and the spherical Cr_2O_3 surface was loose and porous clearly (Figs. 2(e) and 2(f)). Nanostructural CrN electrode materials were obtained by annealing different nanostructural Cr_2O_3 in ammonia atmosphere as shown in the schematic diagram. During the reaction, the oxygen atoms in Cr_2O_3 are replaced by nitrogen atoms, resulting in CrN materials with loose nanostructures. The whole high-temperature ammoniation process is presented by the following formula:

$$Cr_2O_3 + 2NH_3 \rightarrow 2CrN + 3H_2O. \tag{5}$$

By the combination of the construction of Cr_2O_3 nanostructure precursors with the ammoniating process, CrN materials with different nanostructures were obtained. Compared with the morphologies of the Cr_2O_3 precursors, there are the following differences of as-prepared CrN materials. The size of the CrN nanoparticles was reduced and has no clear edges from the observation of TEM test. The surface of the CrN microspheres is looser (Fig. 3(g)), and the CrN is observed as loose microspheres by TEM observation (Fig. 3(h)). In the cross-section, there are a lot of holes in the CrN microlayers (Fig. 3(d)). For CrN nanoparticles, the HRTEM image shows the interplanar spacing of 0.24 nm and 0.21 nm, which is consistent with the cubic CrN (111) and (200) interplanar spacing.[13] For the microlayer and microspherical CrN, the corresponding (200) crystal plane was also found, confirming that high-temperature ammoniation could completely transform transition metal oxides into transition metal nitrides. These unique nanostructures may provide fast transmission channels for electronic transport, thereby improving energy storage performance.

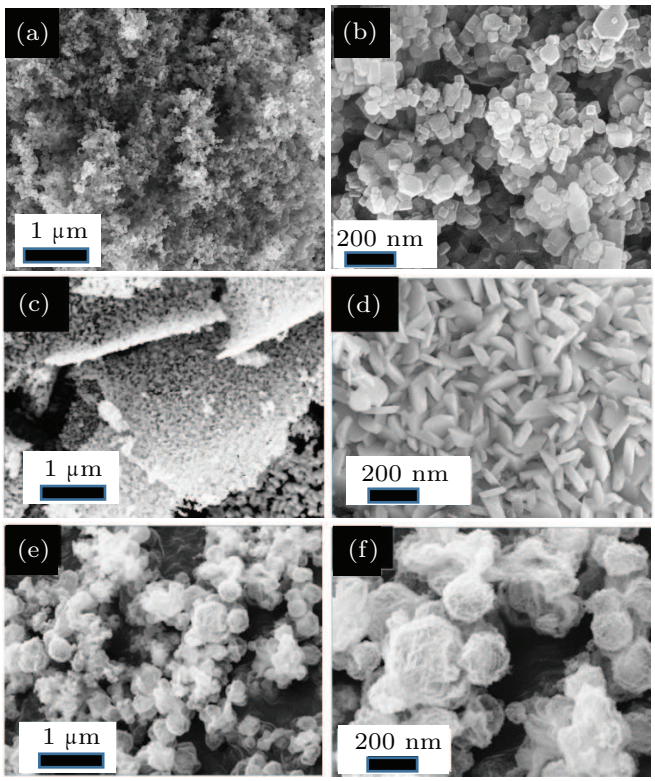


Fig. 2. SEM images of Cr_2O_3 at different magnifications: (a) 10 kx nanoparticles; (b) 50 kx nanoparticles; (c) 10 kx microlayers; (d) 50 kx microlayers; (e) 10 kx microspheres; (f) 50 kx microspheres.

The XRD patterns of CrN nanostructures with different morphologies were shown in Fig. 4(a). The prepared CrN nanostructures have a cubic crystal structure (JCPDS No. 03-065-2899) after hightemperature nitridation.[20,21] High-temperature ammoniation could completely convert hexagonal Cr_2O_3 into cubic CrN, which is consistent with the HRTEM measurement results. Three peaks at 574.5, 575.6,

and 586.5 eV were found in Figs. 4(b) and 4(c), which were attributed to the formation of CrN compounds by the reaction between Cr and N during the nitridation process.[22,23] The peak at 396.6 eV in the N 1s spectrum was derived from the Cr-N bond.[24]

XPS measurements were further employed to analyze the element composition and valence states of the CrN sample. XPS experiments confirmed that there were only two elements, Cr and N, in the synthesized CrN sample, which is consistent with XRD analysis. In the high-resolution XPS scan, Cr 2p core splits into 2p 3/2 and 2p 1/2 peaks (575.5 eV and 584.9 eV). The results indicated that Cr element exhibited +3 oxidation states in the sample. On the other hand, N 1s peak was fitted into 396.6 eV, and indexed to the Cr-N bond.[22–24]

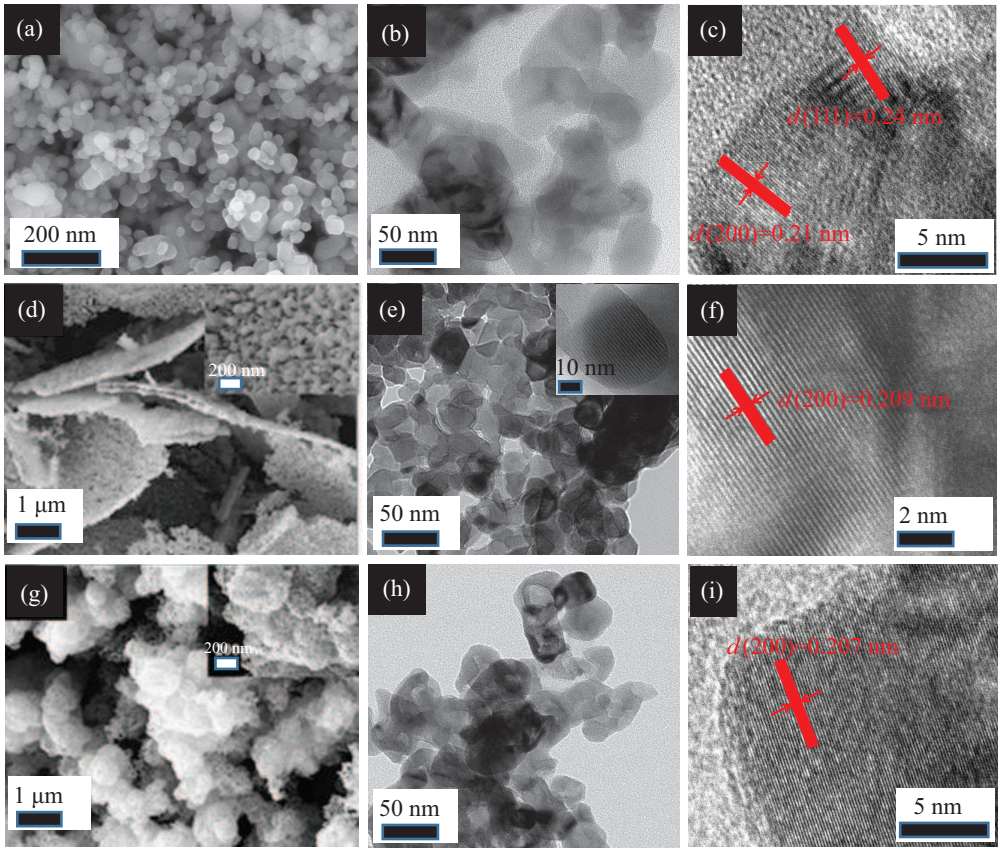


Fig. 3. Morphologies of CrN nanoparticles: (a) SEM, (b) TEM, (c) HRTEM. Morphologies of CrN microlayers: (d) SEM, (e) TEM, (f) HRTEM. Morphologies of CrN microspheres: (g) SEM, (h) TEM, (i) HRTEM. The insets at the upper right of figures [panels (d), (e), (g)] show the magnified view.

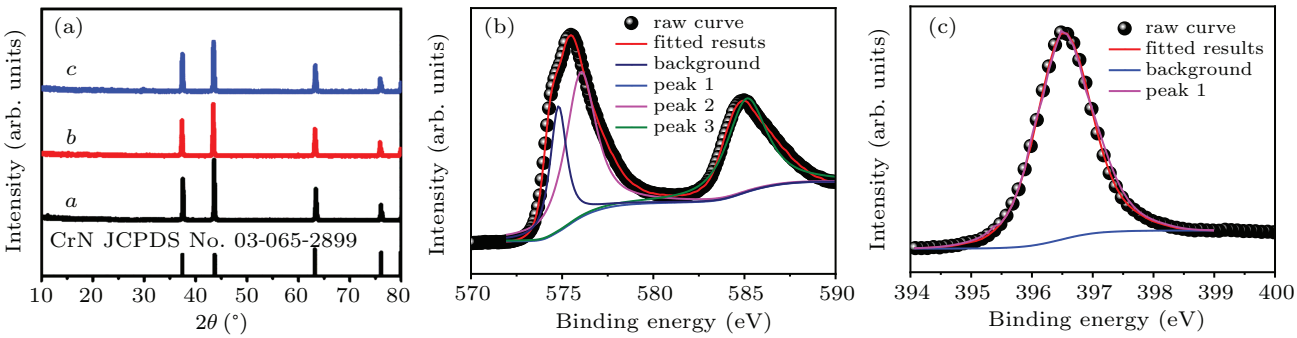


Fig. 4. (a) XRD patterns of CrN with different nanostructures: nanoparticles (black line), microsphers (red line), and microlayers (blue line). XPS spectra of CrN with (b) Cr 2p and (c) N 1s.

Initially, CrN materials with different morphologies were evaluated by the cyclic voltammetry and current charge-discharge curves in Fig. 5. It could be seen that the rectangular area of the CV curve of the CrN nanoparticles was small at different scan rates, resulting in its small capacitance. By combining with the GCD curve, it could be seen that there is oxidation–reduction reaction during the charge and discharge process. For the microlayered CrN, the CV curve is almost rectangular and has a weak redox peak. Combined with the GCD curve results, it shows that there is a redox pseudocapacitance behavior during the electrochemical behavior. Figure 5(e) shows the CV curve of porous spheri-

cal CrN. The redox peak was found obviously, indicating that there is a redox pseudocapacitance behavior during the electrochemical charging and discharging process, which is consistent with the result of the GCD curve. According to the CV and GCD curves, the specific capacitance of the electrode material was calculated (Eqs. (1) and (2)). The specific capacitance decreases with the increase of the scan rate, as CrN electrode material showed a slow transfer and charge diffusion in the KOH electrolyte at a higher scan rate. Within the scan rate range of 10 mV/s–500 mV/s, the specific capacitance drop range of CrN nanoparticles, microlayers, and microspheres were: 82.4 F/g→55.6 F/g, 126.7 F/g→63.2 F/g, 213.2 F/g→106.3 F/g respectively, and the corresponding specific capacitance retention rates were 67.5%, 49.8%, and 49.9%, respectively.

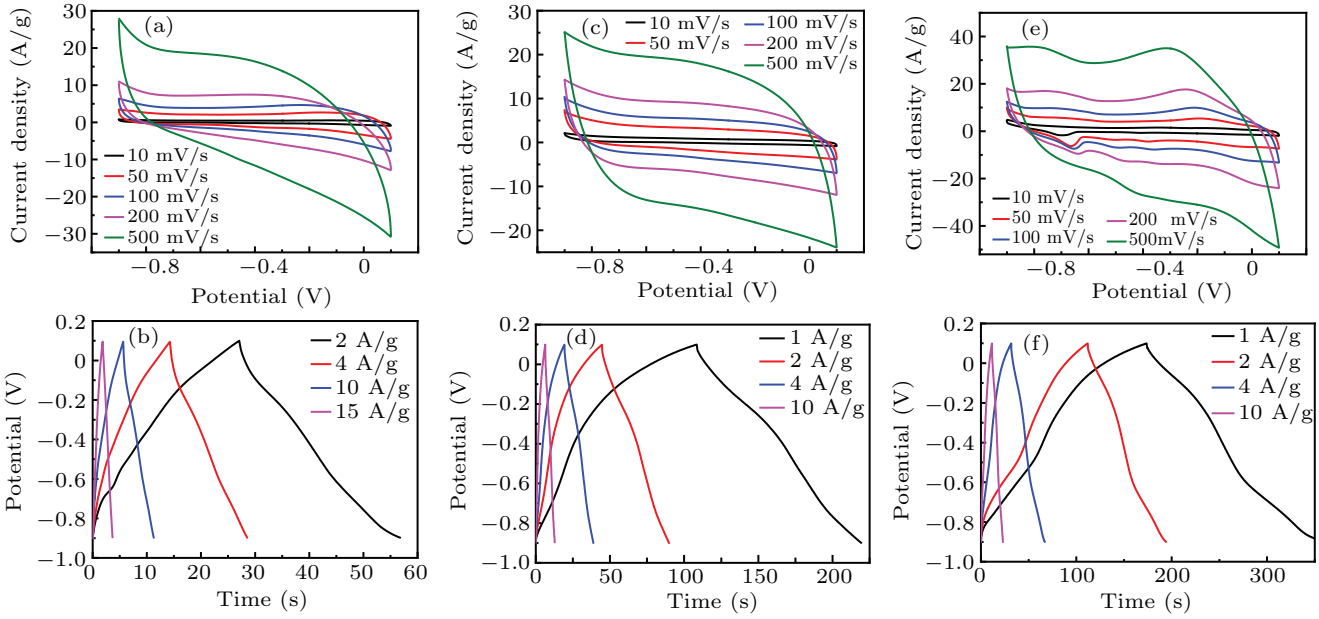


Fig. 5. The CV and GCD curves of CrN with different morphologies: (a) nanoparticles CV, (b) nanoparticles GCD, (c) microlayers CV, (d) microlayers GCD, (e) microspherical CV, and (f) microspherical GCD.

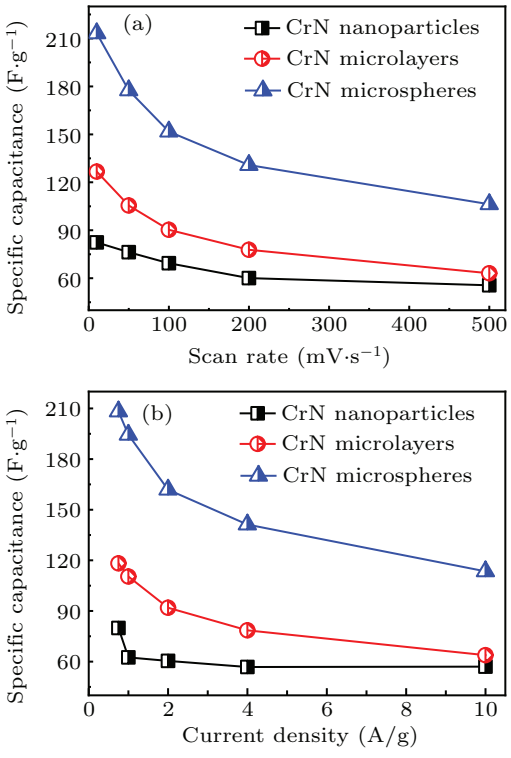


Fig. 6. Specific capacitance of CrN with different nanostructures under (a) different scanning rates and (b) different current densities.

The relationship between current density and specific capacitance was shown in the curves of Fig. 6. As the current density increases, the specific capacitance gradually decreases, which is consistent with the trend between the scan rate and specific capacitance curve. In the current density range of 0.75 A/g–10 A/g, the specific capacitance drop intervals of CrN nanoparticles, microlayers, and microspheres were 79.8 F/g→55.0 F/g, 118.0 F/g→63.8 F/g, 208.1 F/g→113.5 F/g, respectively. The corresponding specific capacitance retention rates were 68.9%, 54.1%, and 54.5%, respectively. For the above three different nanostructures of CrN materials, although the CrN nanoparticles had a higher specific capacitance retention rate, the specific capacitance was smaller. In contrast, the porous microspherical CrN had a high specific capacitance with a scan rate of 500 mV/s and 10 A/g, showing a big advantage in the application of supercapacitors.

To probe the conductive property occurring at electrode/electrolyte interfaces, impedance spectra of different nanostructured CrNs were obtained. The impedance curves of CrN nanoparticles, microlayers, and microspheres were approximately vertical, indicating that the three types of CrN

nanostructures all exhibit capacitance characteristics. The intercept between the impedance curve of the sample in the high-frequency region and the X axis can reflect the internal resistance (R_s) of the electrode material. As shown in the insets of Figs. 7(a) and 7(c), the R_s for CrN nanoparticles, microlayers, and microspheres were 1.5 Ω, 2.9 Ω, and 0.9 Ω, respectively. Among them, the internal resistance of microlayer CrN was the largest, due to a large number of voids in the cross-section of the microlayered CrN. For microspheres CrN, R_s is significantly smaller than that of other nanostructures, proving porous spherical CrN has the best conductive property. It was even smaller than that of TMOs electrode materials, such as Cr_2O_3 ($R_s = 2.3$ Ω),[25] MoO_3 ($R_s = 2.22$ Ω),[26] V_2O_5 ($R_s = 1.3$ Ω).[27]

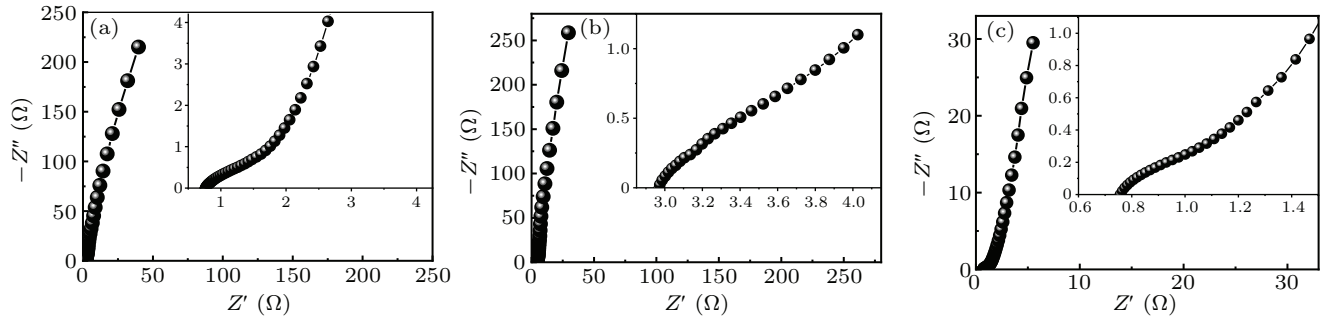


Fig. 7. EIS plots of CrN with different nanostructures: (a) nanoparticles, (b) microlayers and microspheres. The insets display the impedance spectra in the high-frequency region.

Comparing CrN electrode materials with different nanostructures, the specific capacitance was as follows: 82.4 F/g (nanoparticles) > 126.7 F/g (microlayers) < 213.2 F/g (microspheres). They were higher than that of other reported CrN electrodes, such as CrN nanoparticles (75 F/g) and CrN film (41.6 F/g).[11,20] The porous microspherical CrN had the biggest specific capacitance, due to the large specific surface area. According to the results of nitrogen adsorption and desorption (Fig. 8(a)), the specific surface areas of as-obtained CrN nanoparticles, microlayers, and microspheres were 13.7, 28.6, and 58.1 cm^3/g, respectively. Compared with the other two nanostructures, the specific surface area of microspherical CrN was significantly increased. As shown in Fig. 8(b), the capacity retention rate of the porous spherical CrN nanostructure after 5000 cycles in 1-mol/L KOH solution is 96%, demonstrating its excellent cycle stability in strong alkaline electrolytes.

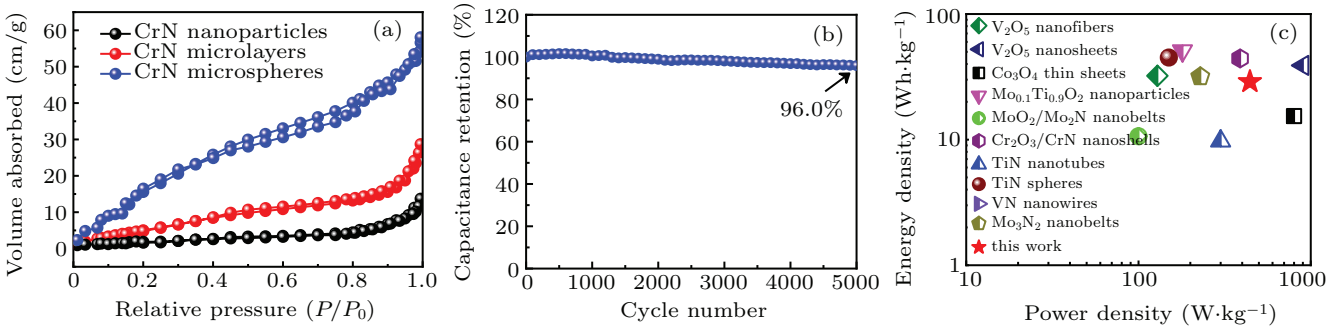


Fig. 8. (a) Nitrogen adsorption–desorption isotherms of CrN with different nanostructures. (b) Cycling stability of CrN microspheres at room temperature. (c) Ragone plot of supercapacitors for CrN microsphers, V_2O_5 nanofibers,[27] V_2O_5 nanosheets,[29] Co_3O_4 thin sheets,[30] $Mo_{0.1}Ti_{0.9}O_2$ nanoparticles,[31] MoO_2/Mo_2N nanobelts,[32] Cr_2O_3/CrN nanoshells,[13] TiN nanotubes,[33] TiN nanospheres,[34] VN nanowires,[35] and Mo_3N_2 nanobelts.[28]

By using the Eqs. (5) and (4), we calculated the power density (443.4 W/kg) and energy density (28.9 Wh/kg) of porous spherical CrN. By comparing the energy density and power density of other metal oxide and metal nitride electrode materials,[27–35] porous microspherical CrN had excellent supercapacitor characteristics (Fig. 8(c)). A large number of studies have shown that electrode materials with different nanostructures exhibit different electrochemical properties. In the samples we constructed, the porous spherical CrN exhibits remarkable electrochemical performance, and the reason was summarized: by the following points: (i) A smaller internal resistance can effectively promote the rapid transfer of charges and shorten the charge and discharge time;[36,37] (ii) The porous microspherical nanostructure has a larger specific surface area and successfully constructed a three-dimensional electrical charge network to further enhance the charge transfer rate.[38]

4. Conclusion

In this work, we provide a new strategy for the design and development of nanostructural CrN electrode materials with different morphologies (nanoparticles, microlayers, and

microspheres). The specific capacitances of the three nanostructured CrNs were: 213.2 F/g (microspheres) >126.7 F/g (microlayers) > 82.4 F/g (nanoparticles). Importantly the capacity retention rate of porous CrN microspheres is 96% after 5000 cycles in 1-mol/L KOH solution, and its energy density and power density reached 28.9 Wh/kg and 443.4 W/kg. These characteristics could effectively improve the energy storage characteristics of the electrode material.

References

[1] Shao Y, El-Kady M F, Sun J, *et al.* 2018 *Chem. Rev.* **118** 9233
[2] Han N, Liu P Y, Jiang J, *et al.* 2018 *J. Mater. Chem. A* **6** 19912
[3] Naik G V, Schroeder J L, Ni X, *et al.* 2012 *Opt. Mater. Express* **2** 478
[4] Haider W A, Tahir M, He L, *et al.* 2020 *ACS Cent. Sci.* **6** 1901
[5] Balogun M S, Zeng Y, Qiu W, *et al.* 2016 *J. Mater. Chem. A* **4** 9844
[6] Kao E, Yang C, Warren R, *et al.* 2016 *Sens. Actuator A Phys.* **240** 160
[7] Lucio-Porto R, Bouhtiyya S, Pierson J F, *et al.* 2014 *Electrochim. Acta* **141** 203
[8] Eustache E, Frappier R, Porto R L, *et al.* 2013 *Electrochem. Commun.* **28** 104
[9] Shah S I U, Hector A L and Owen J R 2014 *J. Power Sources* **266** 456
[10] Wei B B, Liang H F, Zhang D F, *et al.* 2017 *J. Mater. Chem. A* **5** 2844
[11] Das B, Behm M, Lindbergh G, *et al.* 2015 *Adv. Powder Technol.* **26** 783
[12] Wei B B, Mei G, Liang H F, *et al.* 2018 *J. Power Sources* **385** 39
[13] Zhang M, Xiong Z W, Jia J Z, *et al.* 2020 *J. Electroanal. Chem.* **856** 113696
[14] Haye E, Achour A, Guerra A, *et al.* 2019 *Electrochim. Acta* **324** 134890
[15] Shi J, Jiang B L, Li C, *et al.* 2020 *Mater. Chem. Phys.* **245** 122533
[16] Zheng Y, Zhou T F, Zhao X D, *et al.* 2017 *Adv. Mater.* **29** 1700396
[17] Wang C, Zhou P, Wang Z Y, *et al.* 2018 *RSC Adv.* **8** 12841
[18] Hou Z Q, Guo K, Li H Q, *et al.* 2016 *CrystEngComm* **18** 3040
[19] Abdelaal H 2015 *Appl. Sci. Lett.* **1** 24
[20] Xu X Y, Wu J, Yang N, *et al.* 2015 *Mater. Lett.* **142** 172
[21] Zhao L, Wang L, Yu P, *et al.* 2015 *Chem. Commun.* **51** 12399
[22] Subramanian B and Jayachandran M 2011 *Eng. Sci. Technol.* **46** 554
[23] Milošv I, Strehblow H H, Navinšek B, *et al.* 1995 *Surf. Interface Anal.* **23** 529
[24] Wu J B, Lin Y F, Wang J L, *et al.* 2003 *Inorg. Chem.* **42** 4516
[25] Kaltenbrunner M, Adam G, Głowacki E D, *et al.* 2015 *Nat. Mater.* **14** 1032
[26] Cao X H, Zheng B, Shi W H, *et al.* 2015 *Adv. Mater.* **27** 4695
[27] Jiang H, Niu H, Yang X, *et al.* 2018 *Chem. Eur. J.* **24** 10683
[28] Xiong Z W, Yang J, Gao Z P, *et al.* 2020 *Results Phys.* **16** 102941
[29] Nagaraju D H, Wang Q, Beaujuge P, *et al.* 2014 *J. Mater. Chem. A* **2** 17146
[30] Jiang Y Q, Chen L Y, Zhang H Q, *et al.* 2016 *Chem. Eng. J.* **292** 1
[31] Bauer D, Roberts A J, Matsumi N, *et al.* 2017 *Nanotechnology* **28** 195403
[32] Tan Y T, Dong W J, Li Y, *et al.* 2018 *New J. Chem.* **42** 17895
[33] Xia C, Xie Y B, Wang Y, *et al.* 2013 *J. Appl. Electrochem.* **43** 1225
[34] Dong, S M, Chen X, Gu L, *et al.* 2011 *ACS Appl. Mater. Interfaces* **3** 93
[35] Wang R T, Lang J W, Zhang P, *et al.* 2015 *Adv. Funct. Mater.* **25** 2270
[36] Xiao X, Peng X, Jin H Y, *et al.* 2013 *Adv. Mater.* **25** 5091
[37] Peng X, Wang L, Hu L S, *et al.* 2017 *Nano Energy* **34** 1
[38] Yu Z, Tetard L, Zhai L, *et al.* 2015 *Energy Environ. Sci.* **8** 702